Analysis of Force Capacity in Magnetic Bearings and Bearingless Motors from the Perspective of Airgap Space Harmonic Fields *

Anvar KHAMITOV[a], Eric SEVERSON[a]

a University of Wisconsin-Madison, Engineering Drive 1415, 53706 Madison, USA, khamitov@wisc.edu, eric.severson@wisc.edu

Abstract

This paper studies the force creation capabilities of active magnetic bearings (AMBs) and bearingless motors from the perspective of multiple airgap space harmonics/pole-pairs. This approach is analytic-based and is useful in explaining the underlying physics of the machine and conducting force capacity analysis for different numbers of phases/poles. The presented per unit (p.u.) model makes the force capacity results applicable to any motor dimensions and peak airgap field value. An explanation of the force capacity in bearingless motors is provided when only two harmonics are controlled (which is the typical approach in bearingless motor literature) and the relationship between torque, force, and magnetizing field values is identified. Using this relationship, optimal magnetizing field values for maximum torque-force capability are identified, which is useful to consider when designing a bearingless motor. This paper extends the force capacity analysis to bearingless motors with multiple (more than two) controllable space harmonics and proposes that force enhancement can be achieved through the control of the magnitudes and angles of these harmonics. Results show that potential force enhancement of over 40% in bearingless machines can be achieved when controlling four airgap harmonics as opposed to two harmonics. These results suggest that being able to control multiple harmonics can yield high performance designs.

Keywords: active magnetic bearing, bearingless motor, self-bearing motor, current sequences, force enhancement

1. Introduction

Magnetic levitation technologies have been developed as an alternative to contact bearings to provide contact-free and lubricant-free support of the motor shaft, eliminating any point of wear, bearing friction, and contamination issues. AMBs have been successful in many applications over different power and speed levels (Chen et al. 2019). However, their use has been limited by high design cost and large size, which reduces the overall motor power density and increases the total shaft length. Bearingless motors have the potential to solve the issues of AMBs. However, they have only been successfully deployed in low power applications as they cannot yet meet high power requirements. Most of the bearingless motor prototypes discussed in the literature are aimed at low power ratings and only a small number of them have efficiencies exceeding 90%. Both technologies are known to have a lower specific load capacity (Maslen & Schweitzer 2009) than other bearing types. Specific load capacity is calculated by dividing the rated force (maximum force that can be created at any angle) by the projected rotor area (length × diameter) (Chiba et al. 2005). Typically, AMBs have a specific load capacity of 30-40 N/cm^2, with cobalt-alloys reaching up to 65 N/cm^2 (Maslen & Schweitzer 2009, Jastrzebski et al. 2021, Mushi et al. 2011, Swanson et al. 2008). Bearingless motors are often assumed to have a significantly lower load capacity of approximately 9 N/cm^2 (Chiba et al. 2005). In most publications, force creation and control in AMBs is considered in terms of individual poles/teeth. This paper will present an alternate analysis method from the perspective of airgap space harmonics. The paper will extend force capacity analysis to bearingless motors and show how controlling multiple harmonics can be used to design a bearingless motor with equivalent force capacity to AMBs.

The core contributions of this paper are: 1) explanation of the force capacity of AMBs from the perspective of controllable airgap space harmonic fields, 2) explanation of the force capacity in bearingless motors when only two space harmonics are controlled, and 3) enhancement of the force capacity in bearingless motors by controlling multiple airgap space harmonics and comparison to AMB performance limits. Section 2. reviews pole- and space harmonic-based force models and shows relations between controllable harmonic fields, current sequences, and forces. Section 3. uses the harmonic-based model to explain force capacity in AMBs (contribution 1). Section 4. explains torque-force capability and presents force enhancement potential using multiple harmonics (contributions 2 and 3).

2. Force Creation from the Perspective of Airgap Space Harmonic Fields

This section reviews the force creation in AMBs and bearingless motors based on the airgap space harmonic field interactions presented by the authors in Khamitov & Severson (2022) and identifies the relationship with the conventional method of calculating force in magnetic bearings. Section 2.1 reviews the force vector models and Section 2.2 presents the relationship between airgap harmonics, current sequences, and controllable force vectors. The proposed model (2) is used in subsequent sections to calculate the force capacity in AMBs and bearingless motors.

*This work was supported in part by the USA National Science Foundation under Grant #1942099.

2.1 Pole- and Harmonic-Based Force Vector Models

The conventional method of calculating force in AMBs is based around a magnetic equivalent circuit, where the total force is the vector sum of the forces created by individual poles/teeth Maslen & Schweitzer (2009). This model assumes that the field is normal to the tooth surface and is constant over the tooth span. The cross-section of a general AMB with one coil per pole is depicted in Fig.1a. Each pole i can create an attraction force of $F_i = \frac{A}{2\mu_0}B_i^2$, which depends on the square of flux density B_i in tooth i and the tooth surface area A facing the airgap. Under saturation operation, the pole field has a linear relationship with the pole current. When there are n_p equally spaced poles with the same surface area A as in Fig. 1a, the total created total force vector is (1), where $a^{i-1} = e^{\mathrm{j}(i-1)2\pi/n_p}$ indicates the force direction created by pole i.

$$\vec{F} = Fe^{\mathrm{j}\phi} = \frac{A}{2\mu_0}\left(B_1^2 + aB_2^2 + a^2B_3^2 + \ldots + a^{n_p-1}B_{n_p}^2\right) = \frac{A}{2\mu_0}\sum_{i=1}^{n_p} a^{i-1}B_i^2 \tag{1}$$

An AMB can be equivalently viewed as a multiphase winding with m drive connections (m independent currents), as shown in Fig. 1b. This equivalence allows applying the theories used to analyze multiphase windings in bearingless machines (Generalized Clarke Transformation, winding function theory) and studying force creation in AMBs from the perspective of airgap space harmonic fields. Instead of individually viewing each tooth field, the total airgap field can be studied in terms of its spatial harmonic content along the airgap angle α (see Fig. 1c). Each harmonic of order h is expressed as $B_{\mathrm{n},h}(\alpha) = \hat{B}_{\mathrm{n},h}\cos(h\alpha - \phi_h)$ with a magnitude $\hat{B}_{\mathrm{n},h}$ and an angular location ϕ_h/h, and the total field is the sum of all space harmonics present in the airgap. As an example, Fig. 3b shows a plot of the total airgap field and its space harmonics of orders 1-6 along α. Using harmonic field equations and the Maxwell Stress Tensor, it can be shown that the force is created from the interaction between adjacent harmonics h_i and $h_j = h_i + 1$. This is analogous to the force creation in bearingless machines due to torque p and suspension $p_s = p \pm 1$ pole-pairs. When multiple space harmonics are present, the total created force $\vec{F}$ is the vector sum of the forces due to each pair of adjacent space harmonics:

$$\vec{F} = \sum_{h_i=1}^{n_h-1}\vec{F}_{h_i h_j} = k\sum_{h_i=1}^{n_h-1} C_{h_{ij}}\vec{b}_{h_i}^{*}\vec{b}_{h_j}, \quad \text{where } k = \frac{V_r}{2\mu_0 r} \text{ and } C_{h_{ij}} = \left(1 - h_i\frac{\delta_{\text{eff}}}{r}\right)\left(1 + h_j\frac{\delta_{\text{eff}}}{r}\right) \tag{2}$$

where $\vec{b}_{h_i} = \hat{B}_{\mathrm{n},h_i}e^{\mathrm{j}\phi_{h_i}}$ is a vector that represents the field harmonic h_i, k is a constant in terms of the rotor volume V_r and radius r, and $C_{h_{ij}}$ is a factor considering the effect of the tangential field components (δ_{eff} is the effective airgap length). $C_{h_{ij}} \approx 1$ when $h_{i/j}\delta_{\text{eff}} \ll r$. Some of the harmonics in (2) can be directly manipulated through the control of the equivalent current space vectors/current sequences (more details on this in Section 2.2).

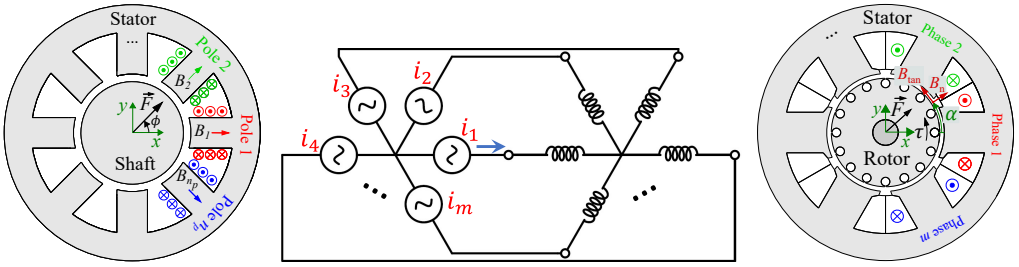

Figure 1: Cross-sections and definitions: (a) an example AMB ($\times$ and $\bullet$ indicate the coil direction into and out of the page, fields are shown for positive currents), (b) multiphase winding circuit diagram, and (c) an example bearingless motor with the definition of axes, fields components, and vectors.

2.2 Relationship to Current Sequences

The concept of current sequences is convenient when studying airgap harmonic fields and forces created from multiphase winding currents. This allows identifying the spatial harmonic content, behavior of created harmonics (rotating or oscillating), and the relationship between the number of independently controllable harmonics and force vector components. This subsection discusses these aspects for AMBs and illustrates using examples. More details on the relationship between harmonics and current sequences are presented in Nishanth et al. (2022) and Khamitov & Severson (2022).

The number of controllable currents m directly determines the number of independently controllable harmonics and their spatial orders. These harmonics can be independently controlled by current sequences. Any set of m-phase currents $\boldsymbol{i} = \begin{bmatrix} i_1 & i_2 & \ldots & i_j & \ldots & i_m \end{bmatrix}^T$ can be decomposed into multiple current sequence components. Phase currents consist of multiple sequences $i_j = i_{j,1} + i_{j,2} + \ldots + i_{j,s} + \ldots$, where a sequence of order s is defined as $i_{j,s} = \hat{I}_s\cos\left(\phi_s - (j-1)s\frac{2\pi}{m}\right)$ with amplitude $\hat{I}_s$, phase angle ϕ_s, and phase separation $s\frac{2\pi}{m}$. Sequence s simultaneously creates harmonics of orders

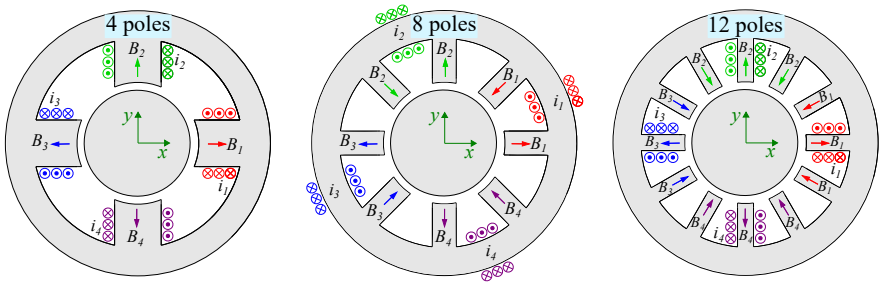

Figure 2: AMBs with 4, 8, and 12 poles (to apply electric motor winding analysis methods, these AMBs can be viewed as each pole wound by a coil).

$h = \pm s + mb$, where b is an integer number. Certain sequences can only control the magnitude of a harmonic (oscillating field), while other sequences can control both the magnitude and angle (rotating field):

$$s = \pm 1,\ \pm 2,\ ...,\ \pm n_{\text{ind}} \text{ control rotating fields, } n_{\text{ind}} = \begin{cases} \frac{m-2}{2} \text{ for } m \in \mathbb{N}_{\text{even}} \\ \frac{m-1}{2} \text{ for } m \in \mathbb{N}_{\text{odd}} \end{cases} \qquad s = 0,\ \frac{m}{2} \text{ control oscillating fields} \tag{3}$$

where n_{ind} is the total number of controllable rotating harmonics. AMBs with $m \in \mathbb{N}_{\text{even}}$ can control two oscillating and $n_{\text{ind}} = \frac{m-2}{2}$ rotating harmonics, while AMBs with $m \in \mathbb{N}_{\text{odd}}$ can control one oscillating and $n_{\text{ind}} = \frac{m-1}{2}$ rotating harmonics.

The force vector model (2) in terms of current quantities can be used to identify the number of controllable force vectors. Using the Generalized Clarke Transformation, current space vector representations of current sequences can be obtained as $\vec{\boldsymbol{i}} = \boldsymbol{C_m i}$ (Wilamowski & Bogdan 2011), where $\vec{\boldsymbol{i}} = \begin{bmatrix} \vec{i}_1 & \vec{i}_2 & ... \end{bmatrix}^T$ is an array of all space vectors. Using the relation between harmonic fields and current sequences, the space vector form of (2) is

$$\vec{F} = \sum_{i=1}^{n_f} \bar{k}_{q,h_{ij}} \vec{i}_i^* \vec{i}_j \tag{4}$$

where $\bar{k}_{q,h_{ij}}$ is the force per ampere squared and n_f is the number of controllable force vectors. This number increases with respect to the number of phases m, which allows for more granular control over the suspension force and potential increase in specific load capacity. To control an individual force vector component $\vec{F}_{h_i h_j} = kC_{h_{ij}} \vec{b}_{h_i}^* \vec{b}_{h_j} = \bar{k}_{q,h_{ij}} \vec{i}_i^* \vec{i}_j$, at least one magnitude and one angle out of four quantities ($\hat{B}_{h_i}$, $\hat{B}_{h_j}$, ϕ_{h_i}, ϕ_{h_j}) must be controllable. This means one harmonic must be able to rotate, while the other harmonic can have a rotating or oscillating behavior. There are $n_{\text{ind}} - 1$ force vectors created independently when controlling all n_{ind} adjacent rotating harmonics. For an even m, an additional force vector can be created when the magnitude of an oscillating harmonic is controlled by sequence $s = 0$ or $\frac{m}{2}$. For an odd m, there is also an additional force vector created by a single sequence of the highest order $s = \frac{m-1}{2}$. This sequence creates two adjacent harmonics of the orders $h_i = s$ and $h_j = -s + m = h_i + 1$, which rotate in opposite directions ($\phi_{h_j} = -\phi_{h_i}$). This explains the way force is created in a three-pole AMB, where harmonics $h_i = 1$ and $h_j = 2$ create force $\vec{F}_{h_i h_j} = kC_{h_{ij}} \hat{B}_{h_i} \hat{B}_{h_j} e^{-2\phi_{h_i}}$. In summary, for any m number of independent winding currents, there are $n_f = n_{\text{ind}}$ independently controllable force vectors.

Consider force creation in 4-, 8-, and 12-pole AMB examples in Fig. 2, where all AMBs have $m = 4$ independent currents. From (3), one rotating harmonic ($n_{\text{ind}} = 1$) from sequence $s = 1$ and one oscillating harmonic from $s = 0$ or $s = m/2$ can be controlled in these AMBs. Controlling one rotating and one oscillating harmonic allows controlling $n_f = 1$ force vector component. The dominant force creating harmonics depend on the winding layout of these AMBs (number of poles per drive connection). Similar to the winding analysis in electric motors, these dominant harmonics can be identified based on their winding factors. The winding factor $\hat{k}_{w,h}$ can take values from zero (harmonic h cannot be created) to one (harmonic h is one of the dominant harmonics). The first dominant harmonic has order $h = n_p/2$ (oscillating), which is created when the subsequent poles in Fig. 2 have alternating magnetic field polarities. In 4- and 12-pole AMBs, this is achieved with $s = 2$ when currents are 180° phase separated (when subsequent currents are equal but opposite). However, in 8-pole AMBs, $h = n_p/2 = 4$ is created by $s = 0$ (all currents are equal). The second dominant harmonic has order of $h = n_p/2 - 1$ (rotating). This harmonic may not be trivial to visualize in 8- and 12-pole AMBs because some of its peaks are not located in front the poles. From the relation $h = \pm s + mb$, this harmonic is created by sequence $s = 1$ in 4- and 12-pole AMBs and by $s = -1$ (negative sequence) in 8-pole AMBs. Since one sequence can create multiple harmonics, sequence $s = \pm 1$ also creates harmonic $h = n_p/2 + 1$ in addition to $h = n_p/2 - 1$, which rotate in opposite directions. If the force equation (2) models one harmonic per sequence (harmonic with the highest magnitude), the interaction between $h = n_p/2 + 1$ and $h = n_p/2$ would be ignored, resulting in force vector error. However, since the control in AMBs is based on individual pole currents instead of particular harmonics, all harmonics (including higher order harmonics) are inherently considered in the force model.

3. Force Capacity of AMBs from the Perspective of Multiple Airgap Harmonic Fields

This section explains the force capacity/design sizing of AMBs from the perspective of multiple airgap space harmonics. This new explanation approach provides insight into identifying and controlling components of the total force vector from each harmonic interaction. The proposed approach to calculate force capacity is explained and the results are presented.

The force vector model in (2) can be used to determine the specific load capacity f_c. The procedure is as follows:

1. Find the maximum force magnitude $F_{\text{max}}(\phi)$ that an AMB can create at every force angle ϕ, while keeping the peak airgap field $\max\left[|B_{\text{n}}(\alpha)|\right] = \max\left[\left|\sum_{h_i=1}^{n_{\text{ind}}} \hat{B}_{h_i}\cos\left(h_i\alpha - \phi_{h_i}\right)\right|\right]$ below the maximum airgap field B_{max}.
2. Calculate the force capacity as $f_c = F_{\text{rated}}/DL$, where $F_{\text{rated}} = \min\left[F_{\text{max}}(\phi)\right]$ is the maximum force that an AMB can create at any force angle ϕ without exceeding the airgap field limit.

To make the force rating and force capacity results applicable to any DL and B_{max} values, a dimensionless form of the force vector model can be used in the above calculations. By setting the base value to $F_{\text{base}} = kB_{\text{max}}^2$, where k is defined in (2), the normalized form of (2) becomes $\vec{F}' = \sum_{i=1}^{n_h-1} \vec{b}'^{*}_{h_i}\vec{b}'_{h_j}$ (assuming $C_{h_{ij}} \approx 1$). Here, each field quantity is normalized by B_{max}. After calculating the normalized rated force F'_{rated} using this model, the force capacity can be calculated as

$$f_c = \frac{kB_{\text{max}}^2 F'_{\text{rated}}}{DL} = \frac{\pi}{4\mu_0} B_{\text{max}}^2 F'_{\text{rated}} \tag{5}$$

This result shows that the force capacity does not depend on DL, but instead depends on the square of the maximum airgap field B_{max} and the harmonics present in the airgap.

This paper shows results of force capacity calculations for AMBs considering only controllable rotating harmonics n_{ind}, resulting in $2n_{\text{ind}}$ control variables. The calculation of the force capacity for $n_{\text{ind}} \geq 2$ has to be solved as an optimization problem as infinitely many solutions exist. Furthermore, the problem has to be solved numerically due to nonlinear objective and constraints. When controlling two rotating harmonics h_i and h_j, the force magnitude and angle of (2) are calculated as $F = kC_{h_{ij}}\hat{B}_{h_i}\hat{B}_{h_j}$ and $\phi = \phi_{h_j} - \phi_{h_i}$. Following the procedure of calculating the specific load capacity, it is found that the rated force of $F'_{\text{rated}} = 0.32$ p.u can be obtained. Substituting this in (5) gives $f_c = 45$ N/cm^2 for $B_{\text{max}} = 1.5$ T (12.8 N/cm^2 for $B_{\text{max}} = 0.8$ T). This result is expected because the force capacity reported in the AMB literature is approximately 40 N/cm^2. Similarly, the force capacity for more than two independent harmonics can be calculated. Figure 3a summarizes the force capacity results for different numbers of harmonics when $B_{\text{max}} = 1.5$ T. This plot shows that an approximately 31% increase in the force capacity can be obtained when increasing n_{ind} from 2 to 6, which is equivalent to increasing the number of poles from 6 to 14 according to (3). As an example, Fig. 3b shows the optimal distribution of the field harmonics when $n_{\text{ind}} = 6$ ($n_p = 14$) to create maximum force along the x-axis. The blue dots indicate the locations of the pole centers. In this case, all harmonics have their peaks located at $\alpha = \phi_{h_i}/h_i = 90^\circ/h_i$, resulting in the total field (indicated with a solid black line) that has better iron utilization. Interestingly, Fig. 3b shows that poles 1 and 8 that are located along the force direction (indicated with a red dashed line at $\alpha = 0$) have zero fields, while three poles on either sides of the force direction (2-4 and 12-14) have the highest field values.

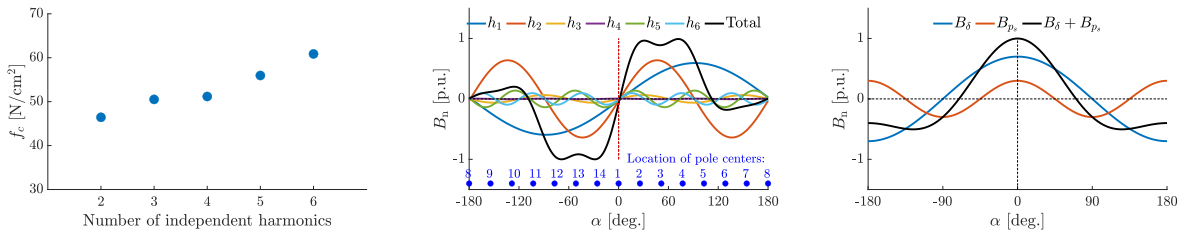

(a) (b) (c)

Figure 3: (a) Results of force capacity analysis in AMBs for different numbers of independent harmonics n_{ind}, (b) optimal airgap field distribution in AMBs for $n_{\text{ind}} = 6$ and $\phi = 0^\circ$, and (c) optimal airgap field distribution in bearingless machines for $n_{\text{ind}} = 2$ and $\phi = 0^\circ$.

4. Force Capacity in Bearingless Motors

This section presents the second and third contributions of the paper. Section 4.1 explains force capacity in bearingless motors when only two space harmonics are controlled, identifies optimal magnetizing field values, and provides an analytical estimation of the torque-force capability using the p.u. model for different magnetizing field values. Section 4.2 proposes potential force capacity enhancement by controlling multiple harmonics. As the primary contribution of this paper, this section finds that, enhancement of force capacity in bearingless machines equivalent to that of AMBs can be achieved through the control of multiple airgap harmonics.

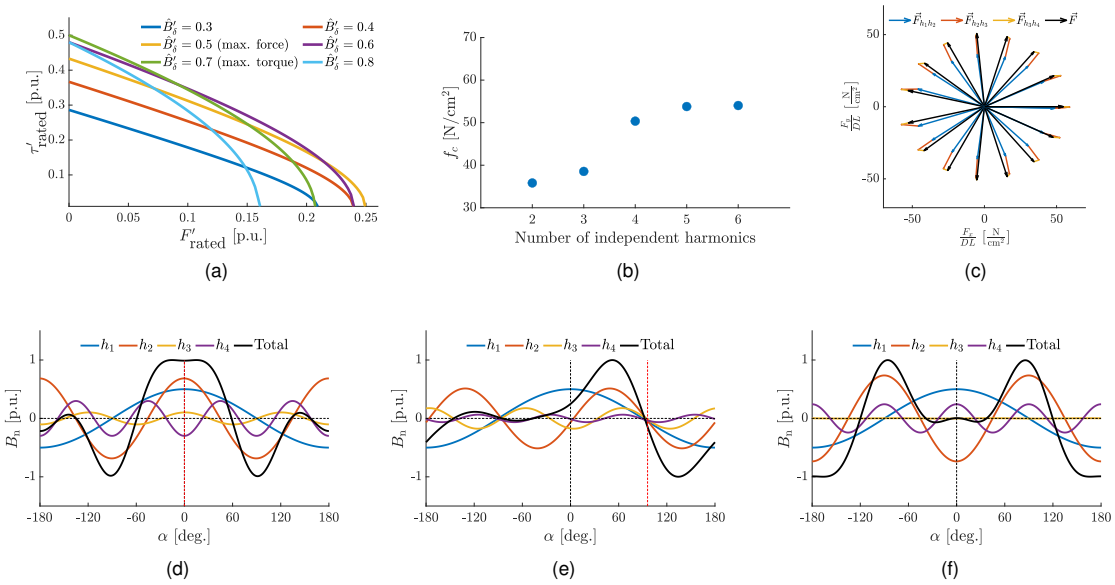

Figure 4: Analysis of force enhancement in bearingless motors: (a) rated torque-force curves for different magnetizing field values when $n_{\text{ind}} = 2$, (b) force capacity vs. number of independent harmonics n_{ind} when $B_{\text{max}} = 1.5$ T and $\hat{B}_\delta = 0.75$ T, (c) optimal force vector components when $n_{\text{ind}} = 4$, and (d)-(f) optimal airgap field distributions for $n_{\text{ind}} = 4$ and $\phi = 0^\circ,\ 90^\circ,\ 180^\circ$.

4.1 Torque-Force Capability from Two Airgap Harmonics

The standard method of creating torque and suspension force in bearingless motors is through controlling p and p_s pole-pair fields. The p pole-pair field consists of a torque creating (q-axis) and a magnetizing field (d-axis) component B_δ, which impacts both torque and force creation. In addition to the force capacity calculation steps described in Section 3. , the magnetizing field harmonic p must have a fixed amplitude at $\hat{B}_\delta$ and an angular location at the rotor rotational angle θ. This subsection identifies the optimal magnetizing field values $\hat{B}_\delta$ when there are two harmonics p and p_s. The optimal magnetizing field is defined as the value creating the maximum force or torque without exceeding the airgap field limit.

First, the optimal $\hat{B}_\delta$ to create the maximum force is identified. With two harmonics in the airgap, the maximum force that can be created at any angle has the magnitude of $F'_{\text{rated}} = \hat{B}'_\delta \hat{B}'_{p_s}$, according to the normalized form of (2). The peak airgap field must not exceed B_{max}, which in p.u. is $\hat{B}'_\delta + \hat{B}'_{p_s} = 1$, as shown in Fig. 3c. Substituting $\hat{B}'_{p_s} = 1 - \hat{B}'_\delta$ gives $F'_{\text{rated}} = \hat{B}'_\delta(1 - \hat{B}'_\delta) = -\hat{B}'^2_\delta + \hat{B}'_\delta$. This is an inverted parabola with the peak $F'_{\text{rated}} = 0.25$ p.u. at $\hat{B}'_\delta = 0.5$ p.u., which gives 35.2 N/cm^2 at $B_{\text{max}} = 1.5$ T and 10 N/cm^2 at $B_{\text{max}} = 0.8$ T. AMBs have approximately 28% higher force capacity at these field values (45 N/cm^2 and 12.8 N/cm^2, see Section 3.) because AMBs do not have the requirement to create the magnetizing field. Now, the optimal $\hat{B}_\delta$ to create the maximum torque is identified. The maximum torque is created when torque creating and magnetizing field components of harmonic p are 90° phase separated electrically, so that $\hat{B}'^2_\delta + \hat{B}'^2_\tau = 1$. The torque is expressed in terms of the normal field components as $\tau_{\text{rated}} = k_\tau \hat{B}_\delta \hat{B}_\tau$, where $k_\tau = V_r p \delta_{\text{eff}} / \mu_0 r$. Defining the base torque value as $\tau_{\text{base}} = k_\tau B^2_{\text{max}}$ (which includes fixed parameters), the normalized form of the torque expression becomes $\tau'_{\text{rated}} = \hat{B}'_\delta \hat{B}'_\tau = \hat{B}'_\delta (1 - \hat{B}'^2_\delta)^{1/2}$. Solving $d\tau'_{\text{rated}} / d\hat{B}'_\delta = 0$, the optimal magnetizing field is found as $\hat{B}'_\delta = 1/\sqrt{2} = 0.707$ p.u. with the maximum $\tau'_{\text{rated}} = 0.5$ p.u. The above calculations show that the optimal magnetizing fields for the maximum force ($\hat{B}_\delta = 0.5$ p.u.) and torque ($\hat{B}_\delta = 0.707$ p.u.) creation are different.

The above analysis can be extended to the case when maximum torque and suspension forces are created simultaneously. In this case, the peak airgap field is constrained by $(\hat{B}'^2_\delta + \hat{B}'^2_\tau)^{1/2} + \hat{B}'_{p_s} = 1$. Using this expression, $F'_{\text{rated}} = \hat{B}'_\delta \hat{B}'_{p_s}$, and $\tau'_{\text{rated}} = \hat{B}'_\delta \hat{B}'_\tau$, the relationship between the rated force, torque, and magnetizing field can be derived:

$$\tau'^2_{\text{rated}} = F'^2_{\text{rated}} - 2\hat{B}'_\delta F'_{\text{rated}} + \hat{B}'^2_\delta (1 - \hat{B}'^2_\delta) \tag{6}$$

This equation can be used to determine torque-force capabilities of a bearingless machine for different magnetizing fields, as demonstrated in Fig. 4a. This plot shows that the optimal range of $\hat{B}'_\delta$ is between approximately 0.5-0.707 p.u. depending on the desired range of τ'_{rated} and F'_{rated}. These results can be used to select a magnetizing field value based on the torque and force requirements when designing a bearingless motor.

4.2 Force Enhancement Using Multiple Airgap Harmonics

This section shows that enhancement of the force capacity can be achieved in bearingless motors by controlling more than two rotating space harmonics. To find the force capacity, a similar approach to that described in Section 3. is used with the additional constraints on the magnetizing field harmonic to have fixed magnitude and angle at any force angle ϕ. This reduces the number of degrees of freedom to $2n_{\text{ind}} - 2$ for bearingless motors as opposed to $2n_{\text{ind}}$ in AMBs.

Analysis results are now presented by comparing bearingless motors with different numbers of controllable airgap harmonics n_{ind}. The results are obtained for $p = 1$ and $\hat{B}_\delta = 0.5$ p.u., with the remaining space harmonics $h = 2, 3, 4, ...$, n_{ind} being used to create force. Figure 4b shows the plot of the force capacity vs. n_{ind} for $B_{\text{max}} = 1.5$ T. This result shows that increasing the number of controllable harmonics from $n_{\text{ind}} = 2$ to $n_{\text{ind}} = 4$ can significantly increase force capacity (by approximately 42%). Figure 4c shows the optimal force vector components from each harmonic interaction required to create F_{rated} at different force angles ϕ for $n_{\text{ind}} = 4$. Figures 4d-4f show the optimal field distributions for this example when $\theta = 0^\circ$ and $\phi = 0^\circ, 90^\circ$, and 180°. An interesting trend is observed from the optimization results: the harmonic peaks are typically aligned or opposite when creating forces at angles 0° and $\pm 180^\circ$, and they all have one intersection point when creating forces at angles $\pm 90^\circ$. Furthermore, at certain angles, additional harmonics are used to improve the total airgap field distribution, but not to contribute to the total force creation. This can be observed in Fig. 4f where the third harmonic is zero and the fourth harmonic is used to reduce the peak airgap field, helping to increase the force capacity.

These results show that, by manipulating the magnitudes and angles of multiple harmonics, force enhancement comparable to AMBs can be achieved, while keeping the peak airgap field below the maximum limit.

5. Conclusion

This paper researches force capacity of AMBs and bearingless motors using multiple airgap space harmonic field interactions. It is found that the key factors affecting the force capacity are the peak allowable airgap field and the distribution of the harmonic fields along the inner bore of the stator. The paper finds that, for the same number of controllable currents, bearingless machines generally have lower force capacity than AMBs due to two main reasons. First, AMBs inherently use more harmonics by individually controlling currents. Second, AMBs do not have the requirement to create the magnetizing field harmonic. This increases the degrees of freedom to find the optimal field distribution in AMBs because harmonic magnitudes and angles do not have to be fixed with respect to the force and rotor angles. It has been identified that the optimal range of the magnetizing field magnitude to have the maximum torque-force capability is between 50% (max force) and 70% (max torque) of the peak airgap field. The paper also showed that, by increasing the number of controllable harmonics and optimally manipulating their magnitudes and angles, enhancement of force capacity in bearingless motors is achievable. The results demonstrate that potential force enhancement of over 40% can be achieved in bearingless machines when controlling four airgap harmonics (10 phases) as opposed to the typical approach of controlling only two harmonics (six phases). For example, with 0.8 T peak field, the force capacity of a bearingless motor can be enhanced from 10 N/cm^2 to 14.3 N/cm^2. Overall, this paper proposes a comprehensive framework for analysis of force creation capabilities in AMBs and bearingless motors, and demonstrates the importance of controlling multiple airgap harmonics for achieving high-performance bearingless motor designs.

References

Chen, J., Zhu, J. & Severson, E. L. (2019), 'Review of bearingless motor technology for significant power applications', *IEEE Transactions on Industry Applications* **56**(2), 1377–1388.

Chiba, A., Fukao, T., Ichikawa, O., Oshima, M., Takemoto, M. & Dorrell, D. G. (2005), *Magnetic bearings and bearingless drives*, Elsevier.

Jastrzebski, R. P., Putkonen, A., Kurvinen, E. & Pyrhönen, O. (2021), 'Design and modeling of 2 mw amb rotor with three radial bearing-sensor planes', *IEEE Transactions on Industry Applications* **57**(6), 6892–6902.

Khamitov, A. & Severson, E. L. (2022), Exact torque and force model of bearingless electric machines, *in* '2022 IEEE Energy Conversion Congress and Exposition (ECCE)', IEEE, pp. 1–8.

Maslen, E. H. & Schweitzer, G. (2009), *Magnetic bearings: theory, design, and application to rotating machinery*, Springer.

Mushi, S. E., Lin, Z. & Allaire, P. E. (2011), 'Design, construction, and modeling of a flexible rotor active magnetic bearing test rig', *IEEE/ASME transactions on mechatronics* **17**(6), 1170–1182.

Nishanth, F., Khamitov, A. & Severson, E. L. (2022), Design of multiphase motor windings for control of multiple airgap fields, *in* '2022 IEEE Energy Conversion Congress and Exposition (ECCE)', IEEE, pp. 1–8.

Swanson, E. E., Maslen, E. H., Li, G., Cloud, C. H. et al. (2008), Rotordynamic design audits of amb supported machinery, *in* 'Proceedings of the 37th Turbomachinery Symposium', Texas A&M University. Turbomachinery Laboratories.

Wilamowski, A. & Bogdan, M. (2011), 'The industrial electronics handbook power electronics', *Taylor and Francis Group* .